

# An Expanded Conformation of Single-Ring GroEL-GroES Complex Encapsulates an 86 kDa Substrate

Dong-Hua Chen,<sup>1,3</sup> Jiu-Li Song,<sup>2,3</sup> David T. Chuang,<sup>2</sup> Wah Chiu,<sup>1</sup> and Steven J. Ludtke<sup>1,\*</sup>

<sup>1</sup>National Center for Macromolecular Imaging Verna and Marrs McLean Department of Biochemistry and Molecular Biology Baylor College of Medicine Houston, Texas 77030

<sup>2</sup>Department of Biochemistry University of Texas Southwestern Medical Center Dallas, Texas 75390

## Summary

Electron cryomicroscopy reveals an unprecedented conformation of the single-ring mutant of GroEL (SR398) bound to GroES in the presence of Mg-ATP. This conformation exhibits a considerable expansion of the folding cavity, with ~80% more volume than the X-ray structure of the equivalent *cis* cavity in the GroEL-GroES-(ADP)<sub>7</sub> complex. This expanded conformation can encapsulate an 86 kDa heterodimeric ( $\alpha\beta$ ) assembly intermediate of mitochondrial branched-chain  $\alpha$ -ketoacid dehydrogenase, the largest substrate ever observed to be *cis* encapsulated. The SR398-GroES-Mg-ATP complex is found to exist as a mixture of standard and expanded conformations, regardless of the absence or presence of the substrate. However, the presence of even a small substrate causes a pronounced bias toward the expanded conformation. Encapsulation of the large assembly intermediate is supported by a series of electron cryomicroscopy studies as well as the protection of both  $\alpha$  and  $\beta$  subunits of the substrate from tryptic digestion.

## Introduction

Chaperonins GroEL and GroES, which are homologs of mitochondrial Hsp60 and Hsp10, respectively, promote proper folding and assembly of proteins (Ellis and van der Vies, 1991; Fenton and Horwich, 2003; Horwich et al., 2006; Martin and Hartl, 1997; Sigler et al., 1998). GroEL is a double-ring complex with two heptameric rings of identical 57 kDa subunits, stacking back to back (Braig et al., 1994; Hendrix, 1979; Hohn et al., 1979). Efficient folding of unfolded proteins has been shown to occur inside the *cis* cavity of GroEL encapsulated by GroES in the presence of Mg-ATP (Weissman et al., 1995). The binding of Mg-ATP and substrate to the unoccupied *trans* ring of GroEL triggers a fast disassembly of the *cis* ring, resulting in the release of a partially or completely folded protein from the *cis* cavity (Rye et al., 1997, 1999). The crystal structure of GroEL-GroES-(ADP)<sub>7</sub> complex (1AON) shows a 2-fold enlarge-

ment of the *cis* over the *trans* cavity to a volume of 175,000 Å<sup>3</sup> (Xu et al., 1997). This volume is theoretically capable of accommodating a globular protein of ~142 kDa beneath the GroES cap, assuming a perfect fit to the available space. However, such a perfect fit is improbable, and the practical mass limit for fully unfolded polypeptides that can be capped by GroES is believed to be ~57 kDa, as shown by both *in vivo* (Houry et al., 1999) and *in vitro* (Sakikawa et al., 1999) studies. For proteins larger than this size limit, for example, an 86 kDa maltose binding protein fusion (Huang and Chuang, 1999) and the 82 kDa mitochondrial aconitase (Chaudhuri et al., 2001), productive folding has been shown to occur by binding the unfolded protein to the uncapped *trans* ring of GroEL.

Since chaperonin-mediated folding can occur *in vitro*, electron cryomicroscopy (also known as cryo-EM) and three-dimensional (3D) image reconstruction have been used as major tools to dissect conformational changes in GroEL that confer productive protein folding. Chemically denatured malate dehydrogenase was first shown by cryo-EM to bind to one end of GroEL, with GroES capping the unoccupied opposite end (Chen et al., 1994). Conformational changes in the *trans* ring affected by the binding of denatured glutamine synthetase to the *cis* ring were also visualized by cryo-EM (Falke et al., 2001a, 2001b, 2005). The en bloc domain movement in the *cis* ring capped by GroES during the chaperonin ATPase cycle was first demonstrated by cryo-EM (Roseman et al., 1996) and was later confirmed by X-ray crystallography (Xu et al., 1997). The ATP-bound states of a GroEL mutant deficient in ATPase activity were also captured by cryo-EM (Ranson et al., 2001).

We have shown previously that GroEL/GroES is essential for promoting the conversion of an otherwise kinetically trapped heterodimeric ( $\alpha\beta$ ) intermediate to the native heterotetrameric ( $\alpha_2\beta_2$ ) decarboxylase (E1) component of the human mitochondrial branched-chain  $\alpha$ -ketoacid dehydrogenase (BCKD) catalytic machine (Chuang et al., 1999; Song et al., 2000; Wynn et al., 2000). Surprisingly, the 86 kDa heterodimeric intermediate was found to be capped by GroES inside GroEL or its single-ring mutant (SR1), as indicated by the protection of both the  $\alpha$  and  $\beta$  subunits of the substrate from protease digestion in the presence of nucleotides (Song et al., 2000, 2003). However, the encapsulation of this large native-like intermediate inside the chaperonin *cis* cavity by GroES has not previously been directly observed in any structural study.

In the present work, we used an ATPase-deficient single-ring mutant (SR398) of GroEL as a model to visualize by cryo-EM the heterodimeric ( $\alpha\beta$ ) intermediate inside its single cavity encapsulated by GroES. More significantly, through an extensive series of structural studies both with and without substrate, we observed a set of conformations exhibiting a previously unobserved structure for the SR398-GroES-Mg-ATP complex, demonstrating *cis*-encapsulation of the  $\alpha\beta$  heterodimer, the largest substrate ever observed inside the SR398-GroES cavity.

\*Correspondence: sludtke@bcm.tmc.edu

<sup>3</sup>These authors contributed equally to this work.

## Results

### Molecular Systems for Cryo-EM Experiments

A single-ring mutant of GroEL, SR398, was used as a model to visualize *cis*-encapsulation of the  $\alpha\beta$  heterodimeric intermediate from the E1 component of the human BCKD complex. The D398A mutation reduces ATPase activity to ~2% of the wild-type (Rye et al., 1997), which allows the formation of stable SR398-GroES-Mg-ATP complex in the presence of Mg-ATP without significant hydrolysis of the nucleotide. In addition, as a single-ring mutant, the potential heterogeneity of *trans*-encapsulation is eliminated. Even if some hydrolysis occurs, single-ring mutants are unable to dissociate from GroES, further promoting the presence of the GroES-capped state. Even with all the above factors promoting the desired state, the system remains heterogeneous, as various states of association with SR398, GroES and substrate will still be present.

We performed cryo-EM and single-particle analysis with multiple-model refinement on four different systems: (1) SR398-GroES-Mg-ATP (substrate free); (2) SR398- $\alpha\beta$ -GroES-Mg-ATP (with the large  $\alpha\beta$  heterodimer); (3) SR398- $\beta$ -GroES-Mg-ATP (with the  $\beta$  subunit only); (4) SR398-Nanogold-labeled  $\beta$ -GroES-Mg-ATP (with the  $\beta$  subunit covalently labeled with Nanogold). We begin by examining the results of the control experiment in the absence of substrate.

### Qualitative and Quantitative Evidence of Heterogeneity

Figures 1A and 1B show typical far-from-focus CCD images of the SR398-GroES-Mg-ATP complex and the SR398- $\alpha\beta$ -GroES-Mg-ATP complex, respectively. Images were generally collected as focal pairs: a first image, at low defocus, producing low contrast but higher resolution data, and a second image, farther from focus with improved contrast but lower resolution and more potential radiation damage. The first, close-to-focus images were used for all two-dimensional (2D) averaging and 3D reconstructions. The second images were used when necessary to assist in locating particles within the first images. In these far-from-focus images, the SR398-GroES-Mg-ATP particles can be directly observed to be qualitatively more hollow than the SR398- $\alpha\beta$ -GroES-Mg-ATP particles.

Careful visual inspection of the data in each case demonstrates some heterogeneity in the particle population. For example, SR398 heptamers with no GroES can be found in both images (arrows in Figures 1A and 1B). In the control experiment with no substrate, three states would be expected: SR398 heptamers without GroES, SR398 heptamers capped with GroES, and free GroES heptamers. Free GroES heptamers are relatively small and are excluded from the particle population based on size and shape.

In order to fully evaluate the particle heterogeneity in the raw images, we have carried out a reference-free 2D image analysis of the particles from the close-to-focus images, as described in the [Experimental Procedures](#) section. The set of particles used for the 2D analysis is a superset of those used for later 3D processing. Subsets of the 2D class averages produced in the absence and presence of substrate are shown in [Figures](#)

1C and 1D, respectively. No symmetry is imposed in this process, and no requirement that the particle images form a coherent 3D structure exists. Thus, these averages are free to exhibit the full heterogeneity of the underlying particle population. Nonetheless, particle images in similar orientations would be grouped in the same class due to their similar appearance. For instance, 7-fold “top views” are clearly observed, as are the 90° rotated “side views” and orientations in-between. In addition to demonstrating a good distribution of different particle views, we also observe unexpected heterogeneity among the class averages in both instances. That is to say, structural variations are observed among particles apparently in the same orientation.

### 3D Reconstruction of SR398-GroES-Mg-ATP Particles with Compositional and Conformational Heterogeneity

One important advantage of single-particle imaging over bulk techniques like crystallography is the possibility of computationally classifying heterogeneous particle images into multiple groups, and performing full 3D reconstructions for each group. Unlike the approach used to generate the reference-free 2D class averages in [Figures 1C and 1D](#), the method we used for 3D reconstruction implicitly incorporates the requirement that groups of class averages form self-consistent 3D structures, and as discussed below, 7-fold symmetry is imposed during the 3D reconstruction.

We first generated a rough starting model ([Figure 2I](#)) from the SR398-GroES-Mg-ATP particles set using the EMAN *startcsym* program. This program produces a rough estimate of the 3D structure based on class averages for only two views of the model: the 7-fold symmetric top view and the pseudomirror symmetric side view. We then added imperceptible random noise to the starting model to produce several virtually identical starting models to seed the multiple-model refinement. Using EMAN's *multirefine* command (Brink et al., 2004), we refined three different models from the heterogeneous SR398-GroES-Mg-ATP particle population. This process also separated the particle population into three groups, each of which was further refined independently to produce the three density maps shown in [Figures 2A–2C](#). The expected structure of SR398 without bound GroES was observed ([Figure 2A](#)). Also as expected, a second reconstruction ([Figure 2B](#), standard conformation) matched the corresponding portion of the GroEL-GroES-(ADP)<sub>7</sub> crystal structure (1AON) (Xu et al., 1997) ([Figure 3](#)). However, the third reconstruction ([Figure 2C](#), expanded conformation) exhibited a dramatic conformational change with substantial expansion of the central cavity. While the overall morphology of the expanded conformation can be related to the standard conformation, this conformation is unlike any known structure in the chaperonin family.

In addition to the expansion of the cavity in the apical domain and the corresponding stretching of the attached GroES, there is a large mass located axially in the equatorial domain ([Figure 2C](#)). Note that a smaller protrusion is also observed in this position in the standard conformation ([Figure 2B](#)) and that this mass is also clearly visible in the reference-free class averages

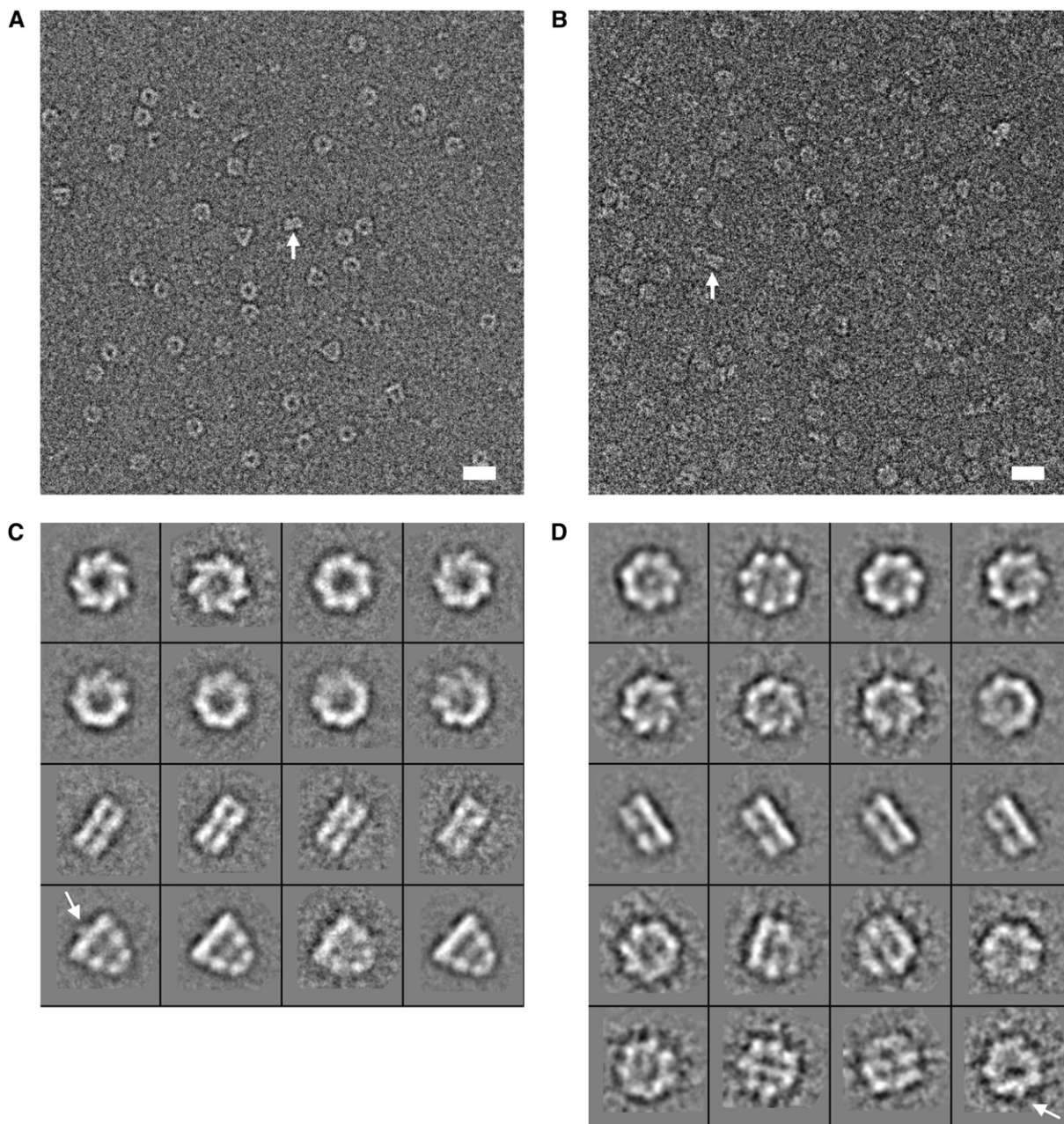


Figure 1. Typical Cryo-Images and Representative Reference-free 2D Class Averages

(A and B) Raw images collected on a Gatan 4k × 4k CCD on a JEOL 2010F electron cryomicroscope (scale bar is 200 Å). The white arrows indicate two particles disassociated from GroES. Both images are the farther-from-focus images from a focal pair and are ~4 μm under focus. (A) The substrate-free SR398-GroES-Mg-ATP complex. (B) The SR398-αβ-GroES-Mg-ATP complex.

(C and D) Representative reference-free 2D class averages generated from the full set of SR398-GroES-Mg-ATP and SR398-αβ-GroES-Mg-ATP images, respectively (31,163 and 24,162 particles respectively). In each case ~300 class averages were generated, a representative subset of which is shown. The number of particles in each class average ranges from ~50 to 150. The first row contains views near the symmetric axis. The second row contains various intermediate tilts. The third row shows side views of particles disassociated from GroES. The 4th and 5th rows contain side views of GroES-associated particles. In both sets, the side views exhibit a clear axial protrusion from the base of the structure, as indicated by the white arrows. There is substantial heterogeneity in the substrate-bound case, so additional representative class averages are shown.

in row 4 of Figure 1C (arrow) and row 5 of Figure 1D (arrow). To explain this, we note that the crystal structure of GroEL excludes 23 residues on the C terminus that were unresolved in the crystal structure (Braig et al., 1994). Recently, modification of this sequence has been successfully used to alter the total volume of the GroEL cav-

ity (Tang et al., 2006). It is tempting to speculate that the observed mass is the portion of this flexible domain lying close enough to the axis for axial averaging to make it visible. Clearly in the presence of the second ring in full GroEL, such mass would be found inside the folding cavity rather than extending outside.

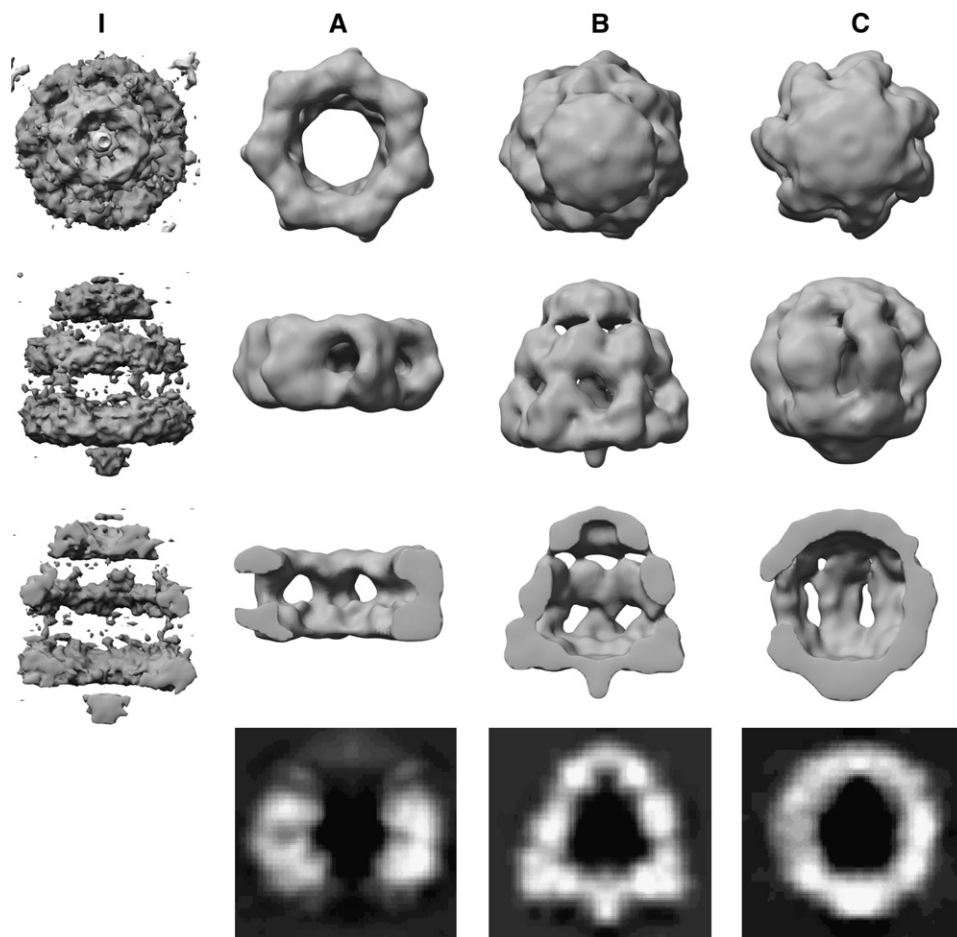


Figure 2. Initial Model and Final Results after Multiple-Model Refinement and Subsequent Single-Model Refinement for the SR398-GroES-Mg-ATP Complex Data

(I) Initial model used to seed the refinement for all three structures. This initial model was generated from the first 6000 particle images of all the data assuming 7-fold symmetry. Perturbative random noise was added to this model to generate the three initial models for the multiple-model refinement since the initial models must not be numerically identical.

(A) SR398 heptamer with no GroES.

(B) Standard conformation.

(C) Expanded conformation. Top row: views along the 7-fold axis; second row: side views, perpendicular to the 7-fold; third row: side views with the front half of the density removed along the 7-fold axis; bottom row: central slices of the density map. Some densities are observable in the slices that are below the isosurface threshold (and thus not observed) in the surface renderings.

Due to the uniqueness of the features revealed in this structure, numerous validation tests (see [Experimental Procedures](#)) were performed to confirm that this novel conformation was authentic, and not an experimental or computational artifact. We estimate that this expanded conformation encloses  $\sim 80\%$  more volume than the equivalent *cis* chamber of the previously determined GroEL-GroES-(ADP)<sub>7</sub> complex (Xu et al., 1997). Much of this increase in volume is due to the transformation from a truncated cone-shaped cavity to an ellipsoidal cavity, meaning this change in volume is accompanied by relatively little change in overall dimensions. Despite the somewhat spherical shape of the expanded state, this conformation has many strong nonspherical features, and structures resembling the intermediate domain of the standard conformation can be observed at corresponding locations in the expanded state. That is, this state does not appear to be produced by any sort of algorithmic error in determining particle orientations.

As shown in the following section, the expanded conformation (Figure 2C) itself is heterogeneous. While the standard conformation (Figure 2B) appears to be a stable, reproducible state, it is possible to subclassify the expanded-state particle images and achieve a variety of subtle structural variations. This indicates that there exists a set of conformations varying between the standard state and the most expanded possible state. Given this heterogeneity and the limited resolution in the expanded state structure, it was not possible to unambiguously model this structure based on the native SR398 structure. Tantalizing surface features reminiscent of the standard conformation are present in the intermediate domain of this structure (Figure 2C), but they are not sufficient to resolve the rearrangements necessary to produce this structure. Nonetheless, this conformation has been validated in numerous ways (see [Experimental Procedures](#)), and expansion of the cavity is clearly occurring.

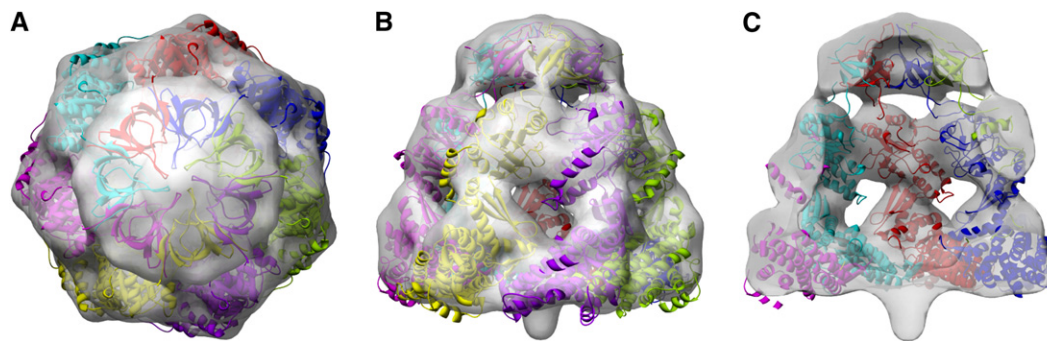


Figure 3. X-Ray Crystallographic Structure of GroEL-GroES-(ADP)<sub>7</sub> with the GroEL *trans* Ring Removed Docked into the Density Map of the Standard Conformation of the SR398-GroES-Mg-ATP Complex

(A) View along the 7-fold axis.

(B) Side view.

(C) Side view with the front half of the density removed along the 7-fold axis. This demonstrates that the standard conformation of the SR398-GroES-Mg-ATP complex agrees well with the known conformation of GroEL-GroES system. Docking was performed using *foldhunter* (Jiang et al., 2001), distributed with EMAN.

To test if this is a peculiarity of this particular single-ring GroEL mutant (SR398), we performed an identical study with the SR1 (Horwich et al., 1998) mutant. Less data were collected in this experiment, resulting in lower resolution, but the results (Figure S1; see the Supplemental Data available with this article online) clearly demonstrate that a similar expanded conformation was observed for the SR1-GroES-Mg-ATP complex.

#### Density Maps of SR398- $\alpha\beta$ -GroES-Mg-ATP

Following the discovery of this novel expanded conformation (Figure 2C) in the absence of substrate, the same analysis techniques were applied to the data collected for the complex in the presence of the  $\alpha\beta$  heterodimer. Several separate multiple-model refinements were performed to address the heterogeneity of the particle population in slightly different ways, and the results were quite self-consistent among these refinements. In the final multiple-model refinement, presented in Figure 4, we used six initial models that focused on the heterogeneity among the expanded conformations. The six initial models included one density map of SR398 in the absence of GroES (Figure 2A), one from the standard conformation of the SR398-GroES-Mg-ATP complex (Figure 2B), and four copies of the map from the expanded conformation of the SR398-GroES-Mg-ATP complex (Figure 2C), each with perturbative random noise added so they were not numerically identical.

Four of the density maps from the final 3D reconstruction are shown in Figure 4, representing one reconstruction (Figure 4A) refined from the standard-conformation model (Figure 2B) and three reconstructions (Figures 4B–4D) refined from the expanded-conformation model (Figure 2C). Another two density maps, representing the single-ring structure disassociated from GroES (Figure S3A) and a heterogeneous structure (Figure S3C), are included in the complete results shown in Figure S3.

The standard conformation (Figure 4A) is very similar in structure to its starting model (Figure 2B), though relatively few particles were found in this conformation. Combined with the inevitable misassignment of a few particles, this structure is of lower quality than the corresponding structure in the substrate-free experiment.

Regardless of quality, this structure demonstrates no evidence of substrate encapsulation. Additional multiple-model refinements were performed to further subclassify the particle images in this conformation, but no evidence for substrate encapsulation was observed in the standard conformation under any conditions.

The other three density maps (Figures 4B–4D) represent the expanded conformations: Figure 4B with no substrate, Figure 4C with some evidence for encapsulated substrate, and Figure 4D with a strong substrate density present. It is clear from the variations in the SR398 and GroES regions of these three density maps that the expanded conformation is not a single rigid conformation, but a heterogeneous particle population representing a range of structures between the standard and fully expanded states. Nonetheless, evidence for substrate encapsulation is obvious.

#### Biochemical Evidence for Substrate Encapsulation

We have shown previously that the partially folded  $\alpha\beta$  heterodimer binds to GroEL as an intact heterodimer, without prior dissociation into individual subunits (Song et al., 2000). To corroborate biochemically that the  $\alpha\beta$  heterodimer is capped by GroES inside the *cis* cavity, protease digestion experiments (Figure 5) were performed using the SR398- $\alpha\beta$  complex. As shown in Figure 5A, in the absence of nucleotide, both  $\alpha$  and  $\beta$  subunits of the heterodimeric intermediate are completely digested both without (Figure 5A, lane 2) and with (Figure 5A, lane 3) GroES. The prominent band under SR398 in the presence of GroES (Figure 5A, lanes 3 and 5) is apparently a proteolytic product of GroEL, since this band is larger than both GroES (migrated close to the dye front and not shown) and the  $\beta$  subunit and does not react with antibodies against either the  $\alpha$  or  $\beta$  subunit (Figure 5B, lane 3). We rationalize that the presence of GroES induces a conformational change in SR398, rendering the latter susceptible to limited tryptic digestion. With Mg-ATP and GroES added, both  $\alpha$  and  $\beta$  subunits are protected from tryptic digestion, resulting from the capping of the SR398 by GroES (Figure 5A, lane 4). No significant protection from tryptic digestion of the  $\alpha$  and  $\beta$  subunits occurs when GroES

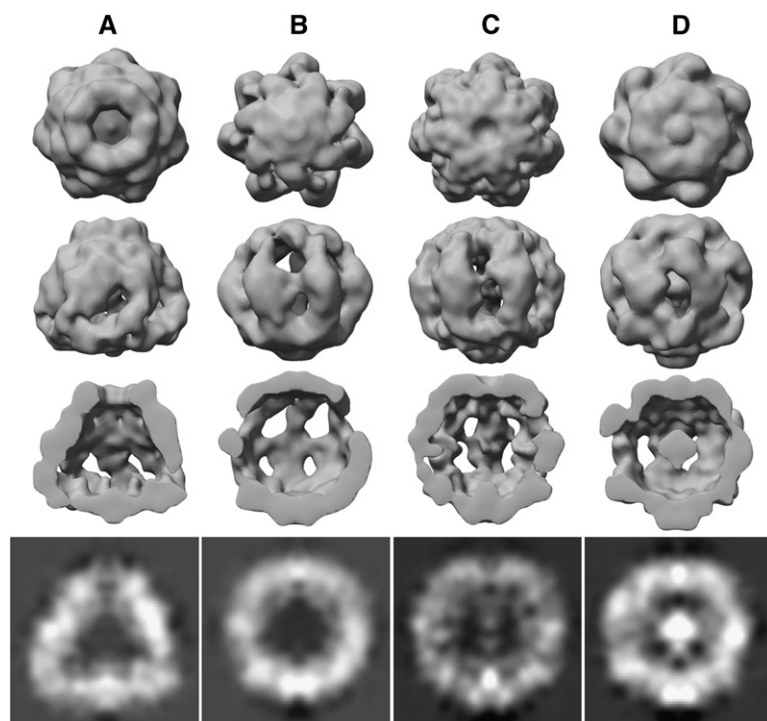


Figure 4. Four Structures Reconstructed by Multiple-Model Refinement and Subsequent Single-Model Refinement for the SR398- $\alpha\beta$ -GroES-Mg-ATP Complex Data

(A) Standard conformation.

(B–D) Three representative expanded conformations. Substrate density is clearly observed inside the folding cavity in (D) and less clearly in (C). Full results with processing intermediates are provided in the [Supplemental Data](#).

and Mg-ADP are present (Figure 5A, lane 5). The identities of the protected  $\alpha$  and  $\beta$  subunits in the SR398 cavity in the presence of GroES and Mg-ATP were established by western blotting (Figure 5B, lane 4). The split band for the  $\alpha$  subunit (Figure 5B, lane 4) suggests a partial exposure of the  $\alpha$  subunit to the protease. Since the  $\alpha$  subunit doublet is not observed with the GroEL double-ring complex (Song et al., 2003), we speculate that the open end

of the equatorial domain in SR398 may not completely prevent the protease from entering the *cis* cavity. The amounts of the protected subunits (Figure 5B, lane 4) are close to those in the starting SR398- $\alpha\beta$  complex (Figure 5B, lane 1), indicating a near complete protection from tryptic digestion. The titer for the  $\beta$  subunit is significantly lower than for the  $\alpha$  subunit, which accounts for the apparently weaker signal for the  $\beta$  subunit compared to the  $\alpha$  subunit with the SR398- $\alpha\beta$  standard (Figure 5B, lane 1). The above results provide the biochemical evidence that 86 kDa heterodimeric  $\alpha\beta$  intermediate is encapsulated by SR398-GroES in the presence of Mg-ATP and therefore protected from tryptic digestion.

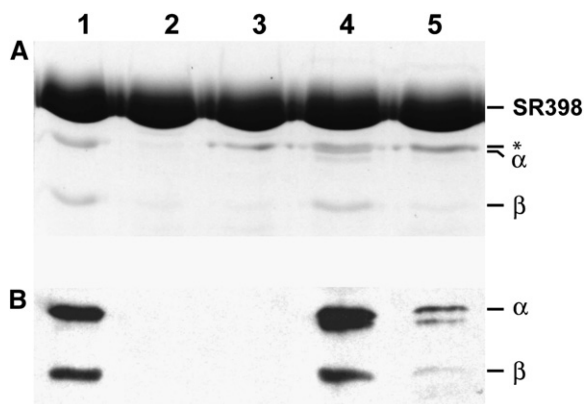


Figure 5. Protection of the 86 kDa  $\alpha\beta$  Heterodimeric Assembly Intermediate from Tryptic Digestion inside the SR398-GroES-Mg-ATP Chaperonin Cavity

(A) SDS-PAGE.

(B) Western blotting.

Combined antibodies to the  $\alpha$  and  $\beta$  subunits were used as a probe. Lane 1, the SR398- $\alpha\beta$  complex; lane 2, the SR398- $\alpha\beta$  complex and trypsin; lane 3, the SR398- $\alpha\beta$  complex, GroES, and trypsin; lane 4, the SR398- $\alpha\beta$  complex, GroES, Mg-ATP, and trypsin; lane 5, the SR398- $\alpha\beta$  complex, GroES, Mg-ADP, and trypsin. The Coomassie blue-stained bands (in lanes 3 and 5) indicated by an asterisk represent a trypsin-digested product of SR398. GroES migrated close to the dye front and is not shown.

#### Structural Evidence for Simultaneous Encapsulation of the $\alpha\beta$ Heterodimer

The structural evidence together with the biochemical evidence presented thus far clearly demonstrates the encapsulation of the  $\alpha\beta$  heterodimer in SR398 cavities. However, accurate mass measurements of the encapsulated density are impossible due to heterogeneity of the system, motion averaging, and residual microscope contrast transfer function (CTF) effects. Based on the previous experiments demonstrating that only proteins smaller than  $\sim 57$  kDa can be encapsulated by the GroEL-GroES complex (Houry et al., 1999; Sakikawa et al., 1999), one concern is that we might be observing  $\alpha$  and  $\beta$  subunits independently encapsulated in the cavity of SR398 by GroES. To directly address this issue structurally, we performed two additional structural studies.

First, the SR398- $\beta$ -GroES-Mg-ATP complex was examined. The data were collected and processed identically to the SR398- $\alpha\beta$ -GroES-Mg-ATP experiment. Results are shown in Figures 6A–6E, with the single-ring structure excluded. These results are very similar to those obtained in the absence of substrate. That is,

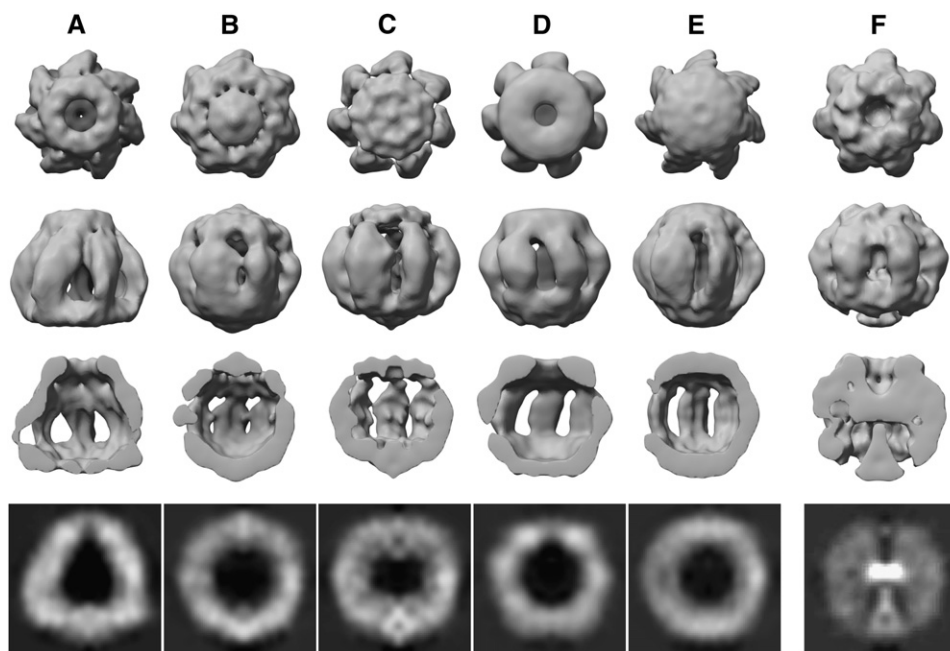


Figure 6. Structures of Five Conformations from the SR398- $\beta$ -GroES-Mg-ATP Complex Reconstructions and One Expanded Conformation from the SR398-Nanogold-Labeled  $\beta$ -GroES-Mg-ATP Complex Reconstructions

(A) Standard conformation of the SR398- $\beta$ -GroES-Mg-ATP complex.

(B–E) Expanded conformations of the SR398- $\beta$ -GroES-Mg-ATP complex.

(F) Expanded conformation of the SR398-Nanogold labeled  $\beta$ -GroES-Mg-ATP complex.

No obvious additional density can be observed in any cavity (A–E) from the SR398- $\beta$ -GroES-Mg-ATP complex. Very strong density from Nanogold-labeled  $\beta$  appeared in the cavity (F) of the SR398-Nanogold-labeled  $\beta$ -GroES-Mg-ATP complex. Despite its clear presence as demonstrated in (F), the  $\beta$  subunit is not directly observed without a Nanogold label.

both standard and expanded conformations are observed, but no clear density is observed inside any of the resulting models. This result could be explained in two ways: either the unfolded  $\beta$  subunit is not encapsulated by SR398, or it cannot be observed in the single-particle reconstruction due to motion averaging of the  $\beta$  subunit within the SR398 cavity.

To distinguish between these possibilities, Nanogold was covalently bonded to the  $\beta$  subunit, and an additional data set was collected for the SR398- $\beta$ (Nanogold)-GroES-Mg-ATP complex. The data were processed in an identical manner to the previous experiments, including use of the same initial models. The expanded conformation exhibiting encapsulated density is shown in Figure 6F. This structure clearly indicates that the  $\beta$ (Nanogold) subunit is encapsulated. Due to the high density of the gold, overall contrast and isosurface levels had to be adjusted so the Nanogold did not overwhelm the protein density.

This observation leaves the question of why the unfolded  $\beta$  subunit is not observed in the density map in the absence of gold. Any system exhibiting the expanded state is still quite heterogeneous, with a variety of subtly different conformations present in the data. Assuming the  $\beta$  chain is moving randomly around inside the cavity, the separation of the data into multiple models may be dominated by changes in overall conformation rather than by the presence or absence of the  $\beta$  subunit density in a random location in the cavity. This results in each of the structures having only a fraction of particle images with the  $\beta$  subunit present. This

effect, combined with residual microscope CTF effects, makes the density of the  $\beta$  subunit effectively undetectable. While the CTF is both amplitude and phase corrected, some small residual effects can generally be observed, and these can make diffuse densities difficult to unambiguously observe. In the experiment with the  $\alpha\beta$  heterodimer, the substrate is massive enough to dominate the classification procedure, and also large enough that, even while moving around the cavity, some mass is always present in the center of the cavity. This theory is further supported by the fact that the encapsulated density is observed only in the center of the cavity. While it is true that the substrate clearly will not exhibit the imposed 7-fold symmetry, and that this will reduce the observed nonaxial substrate densities, if the substrate were consistently binding to a specific binding site on the periphery of the cavity, substantial noncircularly symmetric density would surely be observed.

Additional evidence supporting the existence of the expanded state as well as encapsulation of both substrates is provided by the relative particle fractions observed in each conformation. Table 1 summarizes the relative fractions of GroES-bound particle images found in the standard and expanded conformations in each experiment. In the absence of substrate (Figure 2), the expanded conformation (Figure 2C) represents only 28% of the SR398+GroES population; thus the equilibrium is dominated by the standard conformation (72%) (Figure 2B). The accuracy of these values is bolstered by the independent SR1-GroES-Mg-ATP experiment (Figure S1) with a comparable (29% expanded versus 71%

Table 1. Statistics of GroES-Associated Particles after Multiple-Model Refinement

	Standard Conformation	Expanded Conformation
SR398-GroES-Mg-ATP	72%	28%
SR398- $\alpha\beta$ -GroES-Mg-ATP	20%	80%
SR398- $\beta$ -GroES-Mg-ATP	34%	66%
SR1-GroES-Mg-ATP	71%	29%

standard) ratio. In the presence of the smaller  $\beta$  subunit, the equilibrium shifts strongly toward the expanded conformation (66% expanded versus 34% standard), further confirming its encapsulation. With the larger  $\alpha\beta$  heterodimeric substrate this effect is even stronger (80% expanded versus 20% standard). This explains why it was more difficult to obtain a high-quality standard-conformation structure (Figures 4A and 6A) in the presence of substrate (Figure 2B).

As previously mentioned, 7-fold symmetry was imposed on all of the reconstructions described in this study. At this resolution, 7-fold symmetry is certainly a reasonable assumption for SR398 alone and for the standard conformation of the SR398-GroES-Mg-ATP complex in the absence of substrate. However, there could be some doubt as to whether an expanded conformation of the SR398 complex would remain symmetric. In the presented results, it is clear that there is still considerable heterogeneity in the particles comprising the expanded state. Very likely there are a continuum of intermediates between the standard conformation and the most expanded possible conformation. However, it appears that 7-fold symmetry is a reasonable approximation at the current resolution. Symmetry was not imposed on the 2D class averages in any way, and many reference-free (the first row in Figures 1C and 1D) and reference-based (the first row in Figures S4A and S4B) class averages still exhibit strong 7-fold symmetry. Thus, while we are certainly dealing with a dynamic average, the assumption of 7-fold symmetry is adequate at this resolution to permit a reasonable reconstruction.

Clearly the presence of the encapsulated  $\alpha\beta$  heterodimer will disrupt the 7-fold symmetry, and by imposing the symmetry on this state, we may be averaging out the details of substrate binding to the inside of the GroEL cavity. However, the relatively smooth appearance of the central densities seems to imply that there is, at least, no consistent binding location within the cavity which survives 7-fold averaging.

This loss of information is an unavoidable consequence of the current experimental/computational situation. Due to the level of heterogeneity observed in the SR398- $\alpha\beta$ -GroES-Mg-ATP complex, obtaining a sufficiently homogeneous particle population to reconstruct a specific state without symmetry would require  $\sim 100$  fold increase in the number of particle images. Processing these data would require  $\sim 1000$ -fold more computational power than the present study. While this experiment may become feasible in future, it is simply not possible at the current time. A more likely approach would be to reduce the heterogeneity of the system biochemically, but designing and testing such experimental modifications would also be a substantial undertaking with uncertain prospects for success.

## Discussion

Taken together, the above experiments present a clear picture of the SR398-GroES complex interacting with substrate in the presence of Mg-ATP. The SR398-GroES-Mg-ATP complex in the absence of substrate is capable of considerable expansion (Figure 2C). Observed heterogeneity in the expanded-state structures (Figures 4B–4D) implies that it represents a continuous structural variation comparable to the “breathing” motions observed in some large enzymes (Clare et al., 2006; Kong et al., 2003; Zhou et al., 2001). Due to their dynamic nature, these expanded conformations would not easily be observed in crystallographic studies.

The tryptic digestion experiment that shows protection of the SR398- $\alpha\beta$  complex from tryptic digestion in the presence of GroES and Mg-ATP (Figure 5) supports the conclusion from the cryo-EM experiments that the  $\alpha\beta$  heterodimer is encapsulated by GroES inside the *cis* cavity. Both the tryptic digestion and cryo-EM studies were carried out under the same solution conditions. In an earlier study, we demonstrated that the GroEL (or SR1)- $\alpha\beta$ -GroES ternary complex can be isolated by gel filtration in the presence of Mg-ADP or Mg-ATP, respectively (Song et al., 2003). When these complexes were treated with trypsin, the  $\alpha\beta$  heterodimer was also protected in the presence of appropriate nucleotides. More quantitative studies show that the recovery of both  $\alpha$  and  $\beta$  subunits after protease digestion of GroEL- $\alpha\beta$ -GroES or SR1- $\alpha\beta$ -GroES complex, with all empty cavities blocked by  $\alpha$ -lactalbumin, is equal and better than 80% (Song et al., 2003). Considering the at least 10-fold higher affinity of the  $\beta$  subunit than the  $\alpha$  subunit for GroEL (Song et al., 2000), the only explanation for above data is that both  $\alpha$  and  $\beta$  subunits, existing as a heterodimer, were encapsulated inside the same *cis* cavity of GroEL underneath GroES. As described above, the  $\alpha\beta$  heterodimer binds to GroEL as a single protein with 1:1 subunit stoichiometry (Song et al., 2000). A dissociation of the heterodimer followed by rebinding of individual  $\alpha$  and  $\beta$  subunits to separate GroEL *cis* cavities would have resulted in markedly different levels of protection from the tryptic digestion for the two subunits due to their dissimilar binding affinities for GroEL.

Recently, Motojima et al. reported that, when incubated with polypeptide-bound GroEL or SR1, ADP/GroES failed to produce an efficient reconfiguration of the apical domains to the fully open, GroES-bound position (Motojima et al., 2004). This result explains the fact that full protection of the  $\alpha\beta$  heterodimer is observed only in the presence of Mg-ATP, not Mg-ADP. The 86 kDa native-like heterodimeric  $\alpha\beta$  intermediate in the BCKD assembly pathway represents the largest protein substrate known to fit inside the GroEL *cis* cavity underneath GroES, significantly exceeding the current size limit of  $\sim 57$  kDa established for unfolded proteins (Ewalt et al., 1997; Houry et al., 1999; Sakikawa et al., 1999). The presence of substrate generates a pronounced bias toward the expanded conformation (Table 1), and encapsulated substrate is observed only in the expanded state. As the folding chamber has  $\sim 80\%$  more volume in this conformation than in the standard conformation, the presence of a large substrate like the  $\alpha\beta$  heterodimer

is more reasonable than it would be for encapsulation by the standard conformation.

While the  $\beta$  subunit alone is clearly encapsulated, it is not observed structurally without use of a gold label (Figure 6); however, the  $\alpha\beta$  heterodimer is directly observed in the folding cavity (Figure 4D). The largely central location of the  $\alpha\beta$  heterodimer in the expanded cavity, combined with the difficulty in directly observing the  $\beta$  substrate, implies that the substrate is moving fairly freely within the folding chamber. If there were any specific and strong interactions between substrate and the inner surface of the folding chamber, strong densities would be expected around these points.

Although we would like to speculate on the structural rearrangements producing the expanded state, the present structures represent averages of particle populations that are still heterogeneous. So while the overall shape is representative of the conformational changes experienced by the assembly, some conformational averaging is still occurring. There are features reminiscent of the secondary structure of the intermediate domain of GroEL present in the corresponding domain in the expanded conformation, but the resolution is not adequate to assign locations to specific helices. It appears that the apical and intermediate domains are pulling out, expanding from the center of the structure, causing a stretching of the GroES molecules and the tilting inward of the equatorial domain toward the observed equatorial mass. Elucidation of the details of this conformation is likely to require a large-scale experiment with several hundred thousand particle images subdivided into a large number of subpopulations, such that each subpopulation will be sufficiently homogeneous to achieve subnanometer resolution.

The mammalian mitochondrial chaperonin, Hsp60, exists and functions predominantly as a single-ring rather than a double-ring complex (Nielsen and Cowan, 1998; Nielsen et al., 1999; Viitanen et al., 1992). Thus, while the large expansion observed for SR398 may or may not directly apply to GroEL, it may be an important aspect of single-ring chaperonin behavior. It must be emphasized that the expanded conformation is also observed in the SR1-GroES-ATP complex (Figure S1) and that SR1 converts ATP into ADP at a normal rate. The results argue against the possibility that these conformations result from the prolonged exposure of SR398-GroES to unhydrolyzed ATP. The Anfinsen cage formed by SR1 and GroES is able to promote the complete folding of rhodanese and Rubisco upon a single round of ATP hydrolysis (Brinker et al., 2001; Motojima et al., 2004). Thus, the expanded conformation in the single-ring chaperonin may be of functional significance and may point to a larger degree of flexibility in GroEL structure than previously determined. Previous studies of GroEL were either crystallographic, in which only a single state would be observed, or were single-particle reconstructions assuming from the start that the results would be relatively homogeneous for a particular complex. The current study suggests a new set of experiments on the GroEL-GroES complex and other chaperonin systems to search for previously unobserved conformational variability. It also underscores how common such large-scale motions may actually be, and suggests that more systems should be reinvestigated

structurally, taking possible large-scale motion into account.

## Experimental Procedures

### Preparation of SR398 and Its Complexes

A single-ring GroEL with the D398A mutation (SR398) was produced by QuikChange Site-Directed Mutagenesis Kit (Stratagene, La Jolla, CA) based on the SR1 plasmid kindly provided by Dr. Arthur Horwich. The SR398 protein was expressed and purified using the procedure previously described for SR1 (Song et al., 2003). GroES and the  $\beta$  subunit of BCKD were purified as described previously (Chuang et al., 1999), except the His<sub>6</sub> tag was on the C terminus of the  $\beta$  subunit instead of on the N terminus of the  $\alpha$  subunit. To label the  $\beta$  subunit, 500  $\mu$ l monomaleimido Nanogold reagent (Nanoprobe Inc.; 10 mg/ml) in buffer A (50 mM potassium phosphate [pH 6.0], 150 mM NaCl, 1 mM EDTA, and 8 M urea) was added into 156  $\mu$ l of the  $\beta$ -His<sub>6</sub> subunit (1.4 mg/ml) in the same buffer. After incubation at 23°C for 2 hr, the reaction mixture was diluted 2-fold with buffer A and pH was adjusted to pH 7.5. The  $\beta$ -His<sub>6</sub> subunit was extracted with Ni-NTA resin, and unreacted Nanogold was removed by washing. The Nanogold-labeled  $\beta$ -His<sub>6</sub> subunit was eluted with 250 mM imidazole, and the molar ratio of Nanogold: $\beta$  was measured to be 1.42:1. The SR398- $\alpha\beta$ , SR398- $\beta$ , and SR398-Nanogold- $\beta$  complexes were prepared according to published procedures (Song et al., 2003).

### Tryptic Digestion

In the tryptic digestion experiments, the SR398- $\alpha\beta$  complex (0.86 mg/ml) was incubated with GroES (0.36 mg/ml) in the presence and absence of 3.5 mM nucleotide, followed by tryptic digestion (11  $\mu$ g/ml trypsin) at 23°C for 10 min. After termination of the digestion with 27  $\mu$ g/ml of a trypsin-chymotrysin inhibitor (Sigma), the digestion mixture was subjected to SDS-PAGE or western blotting with combined antibodies to the  $\alpha$  and  $\beta$  subunits as probe.

### Electron Cryomicroscopy

The individual components were mixed at room temperature immediately before vitrification to produce the complexes of SR398-GroES-Mg-ATP, SR398- $\alpha\beta$ -GroES-Mg-ATP, SR398- $\beta$ -GroES-Mg-ATP, SR398-Nanogold-labeled  $\beta$ -GroES-Mg-ATP, and SR1-GroES-Mg-ATP, with each at the final protein concentration of about 0.5 mg/ml. The molar ratio between the SR398 (or SR398- $\alpha\beta$ , SR398- $\beta$ , and SR398-Nanogold-labeled  $\beta$ ) or SR1 and the GroES in these complexes was approximately 1:0.9. The final Mg-ATP concentration is approximately 2.5 mM.

Approximately 3  $\mu$ l of sample solution was applied onto each quantifoil grid (R2/1, Quantifoil Micro Tools GmbH, Jena, Germany) and was plunge-frozen into liquid ethane using a fully automated vitrification device (Vitrobot, FEI Company). The frozen hydrated specimens were kept at -178°C in a Gatan cryo-specimen holder (model 626) in a JEM2010F electron cryomicroscope operated at 200 kV. All images were recorded on a Gatan 4k  $\times$  4k 15  $\mu$ m-per-pixel CCD, except SR1-GroES-Mg-ATP images were recorded on Kodak SO-163 films and were scanned on a Zeiss SCAI scanner at 7  $\mu$ m/pixel, averaged 1.5 $\times$  to produce data at  $\sim$ 2.1  $\text{\AA}$ /pixel. Images were collected as focal pairs at 50,000 $\times$  (effective magnification 69,220 $\times$  on CCD) with a dose of  $\sim$ 15 electrons/ $\text{\AA}^2$  per exposure.

### Single-Particle Image Processing

Reference-free 2D class averages (Figures 1C and 1D) were prepared using the *refine2d.py* program in EMAN, which, while in common use, has not been previously described. The first stage of this process is preparing some initial "low-quality" class averages through classifying values calculated from rotational and radial harmonics of the power spectrum of the particles. When properly combined, these values are nearly invariant with respect to particle rotation/translation within the box. This classification eliminated the need for 2D alignment of the particles in this first step and bootstraps the subsequent iterative procedure. Particles in each class are mutually aligned in 2D and averaged together to produce an initial small set ( $\sim$ 10–20) of class averages. These initial class averages will represent a portion of the variation present among the particle data, but

are not representative of the full range of orientations and conformations among the particles.

The first step in the iterative refinement of the class averages is to perform singular value decomposition (SVD) on the class averages (equivalent to multivariate statistical analysis in this context). This process determines the most significant density variations between the images and provides a mathematical basis for classifying particles based only on their most important features. This process has been used for years in the single-particle processing field (Frank, 2006), but in this case, rather than applying SVD to the raw particle images, the Eigen images are determined from class averages. For this to provide useful results, the class averages must first be consistently aligned to one another in 2D. So, before applying SVD, similar class averages are aligned to one another. Each raw particle image is aligned to the best matching class average and then projected into the mathematical subspace defined by a user-specified number of Eigen images from the SVD analysis of the previous class averages. K-means classification (Frank, 2006) is then applied to the projections of the raw particles. This classification is much more accurate than the initial classification step, since it is based on the most important features as determined by SVD, and the particles can now be separated into the final number of groups (in this case ~200–300 averages) rather than just the initial 10–20. Classified particles are then averaged to produce a new set of class averages, which seed the SVD analysis for the next iteration. The process is typically iterated 8–10 times, finally producing a set of class averages representative of the particle views present in the particle set, but with dramatically reduced noise. The final images represent (optionally CTF-corrected) averages of the raw particle data. SVD is used only for particle classification and was not used to “filter” the particles in any way. The resulting class averages span all variations present in the data regardless of source. That is, variations due to orientation and those due to multiple conformations will both be represented in the final averages.

Single-model refinement has been described in detail previously (Ludtke et al., 1999, 2004), and multiple-model refinement was explained previously (Brink et al., 2004). Briefly, in both cases individual particles are first selected from each image. CTF parameters are determined and used immediately to perform phase-flipping corrections, then stored for later amplitude correction. Particles are classified based on their similarity to each of a set of projections of a reference model. CTF-corrected averages are then generated for individual particle classes, which are then used to construct a new 3D model. The process is iterated until it converges. If the structure is self-consistent, the class averages and corresponding projections will be identical except for differences in noise level and slight rotational averaging due to the angular step between projections.

In multiple-model refinement, which was originally developed to examine the conformational dynamics of fatty acid synthase (Brink et al., 2004), the same general procedure is followed, except *N* 3D starting models are provided, and each particle is classified based on not only orientation, but also which of the *N* models it best matches. Therefore, each particle is associated with a single projection of one of the *N* models. This produces *N* sets of CTF-corrected class averages, which are then used to produce *N* new reference models. This process is also iterated until some level of stability is achieved; for example, the number of particles in each set no longer changes significantly (though some specific particles may still move between classes).

When the multiple-model refinement is complete, typically a set of *N* single-model refinements is performed using the particle images associated with each of the *N* models. If the overall process is successful, the structure produced by single-model refinement of each data subset will produce structures consistent with those produced by the multiple-model refinement, though generally at higher resolution. An example of the complete processing sequence applied to the SR398- $\alpha$  $\beta$ -GroES-Mg-ATP complex is shown in Figure S3. This overall process is very computationally intensive. The work described in this study required a total of well over 100,000 CPU-hours (10 CPU-years) on an Athlon-based Linux cluster.

Resolution of the various reconstructions (Table S1) varied from ~11 to 27 Å based on the 0.5 threshold criterion (Böttcher et al., 1997; Ludtke et al., 2001) of the Fourier shell correlation coefficient

(van Heel, 1987); however, with one exception all structures were low-pass filtered to 20 Å for uniform comparison. The exception is the SR1-GroES-Mg-ATP complex (Figure S1) density maps, which had lower resolution and were filtered to ~27 Å resolution.

#### Validation of the Expanded Conformation of the SR398 Complex

One requirement for a robust reconstruction is having a reasonable distribution of particle orientations. Ideally this distribution would be completely uniform, meaning particle orientations are completely random. Certain subsets of orientations could be excluded without compromising the completeness of the model; however the orientation distribution of particle images of both states of the SR398-GroES-Mg-ATP complex is, in fact, reasonably uniform (Figures S4C and S4D).

To further substantiate the expanded conformation, a crossvalidation test was performed between the standard conformation (Figure 2B) and the expanded conformation (Figure 2C) of the SR398-GroES-Mg-ATP complex. In this test, the two GroES-associated models were re-refined with a strong bias toward an incorrect structure. When performing single-particle reconstruction, two inputs are required: the set of particle images and an initial guess at the 3D structure. The initial 3D structure can bias the results of the refinement in cases where the data are heterogeneous or too noisy to converge to a unique structure. To demonstrate that this sort of procedural bias was not occurring in our results, we performed a cross-validation (Figure S2). The refinement of the standard conformation was seeded with the initial 3D model of the expanded conformation, and the data from the expanded conformation were refined using the standard conformation model as a starting point. These tests strongly bias each refinement and provide strong evidence that the 3D density maps are not the results of initial model bias and are truly representative of the data. In both cases, the final refined structure matched the data, not the initial model. That is, the standard-conformation data were refined to a standard-conformation structure and the expanded-conformation data were refined to an expanded-conformation structure, regardless of the initial 3D model. Combined with the typical convergence criteria used to judge the veracity of single-particle reconstructions, this is very strong evidence that the expanded conformation is valid and that the multiple-model refinement technique was correctly classifying the raw particle images.

Crossvalidation tests were also performed on the expanded conformation (Figure 4D) with significant substrate density inside the cavity, using both the standard conformation (Figure 4A) and the completely empty, expanded conformation (Figure 4B) as initial models. While there are clear indications that these data sets retain some structural heterogeneity, in both cases an expanded conformation with significant internal substrate density was still obtained.

As a final confirmation that our structures are indeed representative of the data, we compared projections of the final reconstruction with both the reference-free class averages as shown in Figures 1C and 1D and the class averages produced during the 3D reconstruction. A self-consistent model will produce projections and class averages, which agree except for the higher noise level present in the class averages. The similarity between projections and class averages of the expanded conformation of the SR398-GroES-Mg-ATP complex demonstrates that the expanded conformation is indeed representative of actual views present in the specimen (Figure S4B). The class averages in Figure 1C and 1D are not amplitude CTF-corrected, causing some intermediate-resolution features to be exaggerated as compared with the 3D projections. Also note that Figures 1C and 1D shows only a fraction of the ~300 class averages produced by the iterative reference-free classification algorithm. Overall, there is good qualitative agreement between 2D and 3D analyses.

#### Fitting Crystal Structures into Cryo-EM Density Maps

*Foldhunter* (Jiang et al., 2001) was used to fit the cryo-EM density map of the standard conformation from the SR398-GroES-Mg-ATP complex to the crystal structure of GroEL-GroES-(ADP)<sub>7</sub> (1AON) with the lower GroEL single ring removed. Attempts were also made to dock component domains of the subunit crystal structure into expanded-state models with no successful results.

### Visualization

*Chimera* (Goddard et al., 2005) was used for visual analysis of the 3D structures and to produce all of the surface representations of cryo-EM density maps.

### Supplemental Data

Supplemental Data include four figures and one table and are available at <http://www.structure.org/cgi/content/full/14/11/1711/DC1/>.

### Acknowledgments

This work was supported by NIH grants (P41RR02250, P01GM064692, PN2EY016525, and DK26758) and the Welch Foundation grant I-1286. The authors would like to thank Matthew Baker for his help fitting the crystal structure into the cryo-EM density map.

Received: May 18, 2005

Revised: September 14, 2006

Accepted: September 19, 2006

Published: November 14, 2006

### References

Böttcher, B., Wynne, S.A., and Crowther, R.A. (1997). Determination of the fold of the core protein of hepatitis B virus by electron cryomicroscopy. *Nature* **386**, 88–91.

Braig, K., Otwinowski, Z., Hegde, R., Boisvert, D.C., Joachimiak, A., Horwich, A.L., and Sigler, P.B. (1994). The crystal structure of the bacterial chaperonin GroEL at 2.8 Å. *Nature* **371**, 578–586.

Brink, J., Ludtke, S.J., Kong, Y., Wakil, S.J., Ma, J., and Chiu, W. (2004). Experimental verification of conformational variation of human fatty acid synthase as predicted by normal mode analysis. *Structure* **12**, 185–191.

Brinker, A., Pfeifer, G., Kerner, M.J., Naylor, D.J., Hartl, F.U., and Hayer-Hartl, M. (2001). Dual function of protein confinement in chaperonin-assisted protein folding. *Cell* **107**, 223–233.

Chaudhuri, T.K., Farr, G.W., Fenton, W.A., Rospert, S., and Horwich, A.L. (2001). GroEL/GroES-mediated folding of a protein too large to be encapsulated. *Cell* **107**, 235–246.

Chen, S., Roseman, A.M., Hunter, A.S., Wood, S.P., Burston, S.G., Ranson, N.A., Clarke, A.R., and Saibil, H.R. (1994). Location of a folding protein and shape changes in GroEL-GroES complexes imaged by cryo-electron microscopy. *Nature* **371**, 261–264.

Chuang, J.L., Wynn, R.M., Song, J.L., and Chuang, D.T. (1999). GroEL/GroES-dependent reconstitution of  $\alpha_2\beta_2$  tetramers of human mitochondrial branched-chain  $\alpha$ -ketoacid decarboxylase. Obligatory interaction of chaperonins with an  $\alpha\beta$  dimeric intermediate. *J. Biol. Chem.* **274**, 10395–10404.

Clare, D.K., Orlova, E.V., Finbow, M.A., Harrison, M.A., Findlay, J.B., and Saibil, H.R. (2006). An expanded and flexible form of the vacuolar ATPase membrane sector. *Structure* **14**, 1149–1156.

Ellis, R.J., and van der Vies, S.M. (1991). Molecular chaperones. *Annu. Rev. Biochem.* **60**, 321–347.

Ewalt, K.L., Hendrick, J.P., Houry, W.A., and Hartl, F.U. (1997). In vivo observation of polypeptide flux through the bacterial chaperonin system. *Cell* **90**, 491–500.

Falke, S., Fisher, M.T., and Gogol, E.P. (2001a). Classification and reconstruction of a heterogeneous set of electron microscopic images: a case study of GroEL-substrate complexes. *J. Struct. Biol.* **133**, 203–213.

Falke, S., Fisher, M.T., and Gogol, E.P. (2001b). Structural changes in GroEL effected by binding a denatured protein substrate. *J. Mol. Biol.* **308**, 569–577.

Falke, S., Tama, F., Brooks, C.L., 3rd, Gogol, E.P., and Fisher, M.T. (2005). The 13 angstroms structure of a chaperonin GroEL-protein substrate complex by cryo-electron microscopy. *J. Mol. Biol.* **348**, 219–230.

Fenton, W.A., and Horwich, A.L. (2003). Chaperonin-mediated protein folding: fate of substrate polypeptide. *Q. Rev. Biophys.* **36**, 229–256.

Frank, J. (2006). Chapter 2. In *Three Dimensional Electron Microscopy*, Second edition (New York: Oxford University Press), pp. 145–192.

Goddard, T.D., Huang, C.C., and Ferrin, T.E. (2005). Software extensions to UCSF chimera for interactive visualization of large molecular assemblies. *Structure* **13**, 473–482.

Hendrix, R.W. (1979). Purification and properties of groE, a host protein involved in bacteriophage assembly. *J. Mol. Biol.* **129**, 375–392.

Hohn, T., Hohn, B., Engel, A., Wurtz, M., and Smith, P.R. (1979). Isolation and characterization of the host protein groE involved in bacteriophage lambda assembly. *J. Mol. Biol.* **129**, 359–373.

Horwich, A.L., Burston, S.G., Rye, H.S., Weissman, J.S., and Fenton, W.A. (1998). Construction of single-ring and two-ring hybrid versions of bacterial chaperonin GroEL. *Methods Enzymol.* **290**, 141–146.

Horwich, A.L., Farr, G.W., and Fenton, W.A. (2006). GroEL-GroES-mediated protein folding. *Chem. Rev.* **106**, 1917–1930.

Houry, W.A., Frishman, D., Eckerskorn, C., Lottspeich, F., and Hartl, F.U. (1999). Identification of in vivo substrates of the chaperonin GroEL. *Nature* **402**, 147–154.

Huang, Y.S., and Chuang, D.T. (1999). Mechanisms for GroEL/GroES-mediated folding of a large 86-kDa fusion polypeptide in vitro. *J. Biol. Chem.* **274**, 10405–10412.

Jiang, W., Baker, M.L., Ludtke, S.J., and Chiu, W. (2001). Bridging the information gap: computational tools for intermediate resolution structure interpretation. *J. Mol. Biol.* **308**, 1033–1044.

Kong, Y., Ming, D., Wu, Y., Stoops, J.K., Zhou, Z.H., and Ma, J. (2003). Conformational flexibility of pyruvate dehydrogenase complexes: a computational analysis by quantized elastic deformational model. *J. Mol. Biol.* **330**, 129–135.

Ludtke, S.J., Baldwin, P.R., and Chiu, W. (1999). EMAN: semiautomated software for high-resolution single-particle reconstructions. *J. Struct. Biol.* **128**, 82–97.

Ludtke, S.J., Jakana, J., Song, J.L., Chuang, D.T., and Chiu, W. (2001). A 11.5 Å single particle reconstruction of GroEL using EMAN. *J. Mol. Biol.* **314**, 253–262.

Ludtke, S.J., Chen, D.H., Song, J.L., Chuang, D.T., and Chiu, W. (2004). Seeing GroEL at 6 Å resolution by single particle electron cryomicroscopy. *Structure* **12**, 1129–1136.

Martin, J., and Hartl, F.U. (1997). Chaperone-assisted protein folding. *Curr. Opin. Struct. Biol.* **7**, 41–52.

Motojima, F., Chaudhry, C., Fenton, W.A., Farr, G.W., and Horwich, A.L. (2004). Substrate polypeptide presents a load on the apical domains of the chaperonin GroEL. *Proc. Natl. Acad. Sci. USA* **101**, 15005–15012.

Nielsen, K.L., and Cowan, N.J. (1998). A single ring is sufficient for productive chaperonin-mediated folding in vivo. *Mol. Cell* **2**, 93–99.

Nielsen, K.L., McLennan, N., Masters, M., and Cowan, N.J. (1999). A single-ring mitochondrial chaperonin (Hsp60-Hsp10) can substitute for GroEL-GroES in vivo. *J. Bacteriol.* **181**, 5871–5875.

Ranson, N.A., Farr, G.W., Roseman, A.M., Gowen, B., Fenton, W.A., Horwich, A.L., and Saibil, H.R. (2001). ATP-bound states of GroEL captured by cryo-electron microscopy. *Cell* **107**, 869–879.

Roseman, A.M., Chen, S., White, H., Braig, K., and Saibil, H.R. (1996). The chaperonin ATPase cycle: mechanism of allosteric switching and movements of substrate-binding domains in GroEL. *Cell* **87**, 241–251.

Rye, H.S., Burston, S.G., Fenton, W.A., Beechem, J.M., Xu, Z., Sigler, P.B., and Horwich, A.L. (1997). Distinct actions of cis and trans ATP within the double ring of the chaperonin GroEL. *Nature* **388**, 792–798.

Rye, H.S., Roseman, A.M., Chen, S., Furtak, K., Fenton, W.A., Saibil, H.R., and Horwich, A.L. (1999). GroEL-GroES cycling: ATP and non-native polypeptide direct alternation of folding-active rings. *Cell* **97**, 325–338.

Sakikawa, C., Taguchi, H., Makino, Y., and Yoshida, M. (1999). On the maximum size of proteins to stay and fold in the cavity of GroEL underneath GroES. *J. Biol. Chem.* **274**, 21251–21256.

Sigler, P.B., Xu, Z., Rye, H.S., Burston, S.G., Fenton, W.A., and Horwich, A.L. (1998). Structure and function in GroEL-mediated protein folding. *Annu. Rev. Biochem.* **67**, 581–608.

Song, J.L., Wynn, R.M., and Chuang, D.T. (2000). Interactions of GroEL/GroES with a heterodimeric intermediate during  $\alpha_2\beta_2$  assembly of mitochondrial branched-chain  $\alpha$ -ketoacid dehydrogenase. *cis* capping of the native-like 86-kDa intermediate by GroES. *J. Biol. Chem.* **275**, 22305–22312.

Song, J.L., Li, J., Huang, Y.S., and Chuang, D.T. (2003). Encapsulation of an 86-kDa assembly intermediate inside the cavities of GroEL and its single-ring variant SR1 by GroES. *J. Biol. Chem.* **278**, 2515–2521.

Tang, Y.C., Chang, H.C., Roeben, A., Wischniewski, D., Wischniewski, N., Kerner, M.J., Hartl, F.U., and Hayer-Hartl, M. (2006). Structural features of the GroEL-GroES nano-cage required for rapid folding of encapsulated protein. *Cell* **125**, 903–914.

van Heel, M. (1987). Similarity measures between images. *Ultramicroscopy* **21**, 95–100.

Viitanen, P.V., Lorimer, G.H., Seetharam, R., Gupta, R.S., Oppenheim, J., Thomas, J.O., and Cowan, N.J. (1992). Mammalian mitochondrial chaperonin 60 functions as a single toroidal ring. *J. Biol. Chem.* **267**, 695–698.

Weissman, J.S., Hohl, C.M., Kovalenko, O., Kashi, Y., Chen, S., Braig, K., Saibil, H.R., Fenton, W.A., and Horwich, A.L. (1995). Mechanism of GroEL action: productive release of polypeptide from a sequestered position under GroES. *Cell* **83**, 577–587.

Wynn, R.M., Song, J.L., and Chuang, D.T. (2000). GroEL/GroES promote dissociation/reassociation cycles of a heterodimeric intermediate during  $\alpha_2\beta_2$  protein assembly. Iterative annealing at the quaternary structure level. *J. Biol. Chem.* **275**, 2786–2794.

Xu, Z., Horwich, A.L., and Sigler, P.B. (1997). The crystal structure of the asymmetric GroEL-GroES-(ADP)<sub>7</sub> chaperonin complex. *Nature* **388**, 741–750.

Zhou, Z.H., Liao, W., Cheng, R.H., Lawson, J.E., McCarthy, D.B., Reed, L.J., and Stoops, J.K. (2001). Direct evidence for the size and conformational variability of the pyruvate dehydrogenase complex revealed by three-dimensional electron microscopy. The “breathing” core and its functional relationship to protein dynamics. *J. Biol. Chem.* **276**, 21704–21713.